Sfrp1 inhibits lung fibroblast invasion during transition to injury-induced myofibroblasts

Christoph H. Mayr[1,16], Arunima Sengupta[1,16], Sara Asgharpour[1], Meshal Ansari[1,2], Jeanine C. Pestoni[1], Paulina Ogar[1], Ilias Angelidis[1], Andreas Liontos[3,4], José Alberto Rodriguez-Castillo[5], Niklas J. Lang[1], Maximilian Strunz[1], Diana Porras-Gonzalez[1], Michael Gerckens[1,6], Laurens J. De Sadeleer[1,7], Bettina Oehrle[1], Valeria Viteri-Alvarez[1], Isis E. Fernandez[1], Michelle Tallquist[8], Martin Irmler[9], Johannes Beckers[9,10,11], Oliver Eickelberg[12], Gabriel Mircea Stoleriu[6], Jürgen Behr[6], Nikolaus Kneidinger[6], Wim A. Wuyts[7], Roxana Maria Wasnick[1], Ali Önder Yildirim[1,13], Katrin Ahlbrecht[5], Rory E. Morty[14], Christos Samakovlis[3,4], Fabian J. Theis[2,15], Gerald Burgstaller[1,17] and Herbert B. Schiller[1,13,17]

[1]Comprehensive Pneumology Center (CPC)/Institute of Lung Health and Immunity (LHI), Helmholtz Munich, Member of the German Center for Lung Research (DZL), Munich, Germany. [2]Institute of Computational Biology, Helmholtz Munich, Munich, Germany. [3]Department of Molecular Biosciences, The Wenner-Gren Institute, Stockholm University, Stockholm, Sweden. [4]SciLifeLab, Stockholm, Sweden. [5]Max Planck Institute for Heart and Lung Research, Member of the German Center for Lung Research (DZL), Bad Nauheim, Germany. [6]Department of Internal Medicine V, Ludwig-Maximilians University (LMU) Munich, Member of the German Center for Lung Research (DZL), CPC-M bioArchive, Munich, Germany. [7]Laboratory of Respiratory Diseases and Thoracic Surgery (BREATHE), Department CHROMETA, KU Leuven, Leuven, Belgium. [8]Center for Cardiovascular Research, John A. Burns School of Medicine, University of Hawaii, Honolulu, HI, USA. [9]Institute of Experimental Genetics, Helmholtz Zentrum München, Neuherberg, Germany. [10]German Center for Diabetes Research (DZD e.V.), Neuherberg, Germany. [11]Chair of Experimental Genetics, Technical University of Munich, Freising, Germany. [12]Division of Pulmonary, Allergy, and Critical Care Medicine, Department of Medicine, University of Pittsburgh, Pittsburgh, PA, USA. [13]Institute of Experimental Pneumology, LMU University Hospital, Ludwig-Maximilians University, Munich, Germany. [14]Department of Translational Pulmonology, University Hospital Heidelberg, and Translational Lung Research Center (TLRC), Member of the German Center for Lung Research (DZL), Heidelberg, Germany. [15]Department of Mathematics, Technische Universität München, Munich, Germany. [16]C.H. Mayr and A. Sengupta contributed equally to this work. [17]G. Burgstaller and H.B. Schiller contributed equally to this article as lead authors and supervised the work.

Corresponding author: Herbert B. Schiller (herbert.schiller@helmholtz-munich.de)

Shareable abstract (@ERSpublications)
This single-cell study discovered a transitional cell state that appears early after injury and precedes the generation of myofibroblasts. This cell state is characterised by expression of SFRP1, which inhibits fibroblast invasion in fibrogenesis. https://bit.ly/3uifxmJ

Cite this article as: Mayr CH, Sengupta A, Asgharpour S, *et al*. Sfrp1 inhibits lung fibroblast invasion during transition to injury-induced myofibroblasts. *Eur Respir J* 2024; 63: 2301326 [DOI: 10.1183/13993003.01326-2023].

This article has an editorial commentary: https://doi.org/10.1183/13993003.02188-2023

Abstract

Background Fibroblast-to-myofibroblast conversion is a major driver of tissue remodelling in organ fibrosis. Distinct lineages of fibroblasts support homeostatic tissue niche functions, yet their specific activation states and phenotypic trajectories during injury and repair have remained unclear.

Methods We combined spatial transcriptomics, multiplexed immunostainings, longitudinal single-cell RNA-sequencing and genetic lineage tracing to study fibroblast fates during mouse lung regeneration. Our findings were validated in idiopathic pulmonary fibrosis patient tissues *in situ* as well as in cell differentiation and invasion assays using patient lung fibroblasts. Cell differentiation and invasion assays established a function of SFRP1 in regulating human lung fibroblast invasion in response to transforming growth factor (TGF)β1.

Measurements and main results We discovered a transitional fibroblast state characterised by high *Sfrp1* expression, derived from both *Tcf21*-Cre lineage positive and negative cells. *Sfrp1*$^{+}$ cells appeared early after injury in peribronchiolar, adventitial and alveolar locations and preceded the emergence of myofibroblasts. We identified lineage-specific paracrine signals and inferred converging transcriptional

Received: 19 July 2023
Accepted: 13 Nov 2023

trajectories towards *Sfrp1*$^{+}$ transitional fibroblasts and *Cthrc1*$^{+}$ myofibroblasts. TGFβ1 downregulated SFRP1 in noninvasive transitional cells and induced their switch to an invasive CTHRC1^{+} myofibroblast identity. Finally, using loss-of-function studies we showed that SFRP1 modulates TGFβ1-induced fibroblast invasion and RHOA pathway activity.

Conclusions Our study reveals the convergence of spatially and transcriptionally distinct fibroblast lineages into transcriptionally uniform myofibroblasts and identifies SFRP1 as a modulator of TGFβ1-driven fibroblast phenotypes in fibrogenesis. These findings are relevant in the context of therapeutic interventions that aim at limiting or reversing fibroblast foci formation.

Introduction

Extracellular matrix (ECM)-producing myofibroblasts are a key therapeutic target to combat tissue fibrosis, one of the biggest unresolved clinical problems across most major chronic diseases. Several recent single-cell RNA-sequencing (scRNAseq) studies described distinct subsets of collagen-producing stromal cells in mouse and human lungs with distinct spatial locations and different functions in supporting epithelial repair [1–5]. How this heterogeneity of fibroblast identities leads to different cell states and functions in fibrotic disease is unclear.

Genetic lineage tracing in mouse models provides evidence for an alveolar lipofibroblast-to-myofibroblast switch after lung injury that is reversible during the resolution of transient fibrosis upon completed epithelial regeneration [6, 7]. The heterogeneity of cellular sources for myofibroblasts in lung fibrosis remains the subject of current investigations. Apart from lipofibroblasts, alveolar pericytes are also potential sources of myofibroblasts [8]. Proliferation, evasion of apoptosis and invasive capacity of myofibroblasts are key hallmarks of fibrotic disease, and transforming growth factor (TGF)β is a known master regulator of these processes [9, 10]. A vast amount of literature demonstrates the TGFβ-induced induction of α-smooth muscle actin (ACTA)2 in fibroblasts, the most widely used marker of mature myofibroblasts in tissues. However, fate mapping and immunofluorescence analysis of fibrotic tissues and myofibroblast foci also show that a substantial fraction of fibroblasts is ACTA2^{-} [11, 12], suggesting additional molecular complexity and heterogeneity among injury-activated fibroblasts. A recent single-cell analysis of collagen-producing cells in lung fibrosis revealed CTHRC1 as a specific marker of highly invasive ACTA2^{+} myofibroblasts. These cells occur in both mouse and human lung and occupy fibroblastic foci in idiopathic pulmonary fibrosis (IPF) [1].

The regulation of injury-activated fibroblast states is not well understood and of high clinical relevance. Our study reveals the spatiotemporal evolution of distinct fibroblast states towards Cthrc1^{+} myofibroblasts, highlighting early events of injury-induced fibroblast activation that preceded myofibroblastic differentiation. We discovered a novel SFRP1^{+}/ACTA2^{-} transitional state that is initially noninvasive and only becomes invasive upon TGFβ-driven differentiation towards the CTHRC1^{+} myofibroblast state. We show that SFRP1 modulates TGFβ1-induced fibroblast invasion and RHOA pathway activity, which constitutes a novel pathway with potential for targeting fibrotic disease mediated by myofibroblasts.

Material and methods

For details of the materials and methods, please refer to the supplementary material.

Experimental study design

C57B6 (males or females) mice were treated with 3.5 units·kg^{-1} body mass of bleomycin administered intratracheally. Up to two bleomycin-instilled mice were sacrificed at time points (days 0, 2–14, 21, 28, 35, 56) after instillation and subject to scRNAseq using the Drop-seq platform. Tcf21-lineage labelled (*Tcf21*m-Crem-R26R-tdTomato) mesenchymal cells were analysed using the 10x scRNAseq platform. Two healthy C57B6 mouse lungs were used for SCRINSHOT. Primary human lung fibroblasts (pHLFs) and micro-computed tomography (CT) staged IPF tissues, and data from an integrated IPF cell atlas were used for human validation.

Human tissue and ethics statement

pHLFs of non-chronic lung disease donors were obtained from the CPC-M bioArchive at the Comprehensive Pneumology Center (Munich, Germany). Participants provided written informed consent to participate in this study, in accordance with approval by the local ethics committee of the Ludwig Maximilians University (Germany) (project 333-10). Micro-CT-staged IPF samples were provided from the KU Leuven lung biobank (ethical approval S52174). Samples were derived from explanted lungs, after written informed consent from all patients. Unused donor lungs were included as controls, following Belgian legislation. Three IPF lungs and three controls were included.

Data availability

RNA-seq data were deposited to the Gene Expression Omnibus (GEO) database. The high temporal mesenchymal enriched Drop-seq data can be found with the accession code GSE207851, and the Tcf21-lineage labelled mesenchymal 10x data with the accession code GSE207687. Microarray data of pHLFs (Sfrp1-siRNA knockdown) can be found with the accession code GSE207561.

Results

Heterogeneity of mesenchymal cells at distinct spatial localisations in the lung

The *Tcf21*$^+$ lineage constitutes the lung lipofibroblast population [13]. To study heterogeneity within the *Tcf21*$^+$ and *Tcf21*$^-$ fibroblast lineages, we tamoxifen-labelled *Tcf21*$^+$ cells in lungs at 11 weeks of age using *Tcf21*m-Crem-R26R-tdTomato mice (supplementary figure S1a). *Tcf21* lineage-positive (lin$^+$) cells were indeed found near alveolar type 2 (AT2) cells and alveolar capillaries (supplementary figure S1b). We flow-sorted *Tcf21* lin$^+$ and lin$^-$ stromal cells and performed scRNAseq (n=4 mice, k=12.068 cells), identifying six distinct cell types with different *Tcf21*-lineage proportions (figure 1a and supplementary figure S1c and d). Previously established marker genes [1, 14, 15] were used to annotate clusters (supplementary table S1). All cell type identities expressed type 1 collagen (*Col1a2*) (supplementary figure S2c) and were consistent with previous work [1].

We identified three main *Pdgfra*$^+$ populations (lipofibroblasts, adventitial fibroblasts, *Adh7*$^+$ fibroblasts), two *Pdgfrb*$^+$ populations (smooth muscle cells and pericytes) with highly distinct marker genes and pathway enrichments (figure 1b and c), and *Pdgfra/Pdgfrb* double-positive cells, as recently found in the kidney [16]. These cells expressed *Lgr5* and *Lgr6* (figure 1b), markers for a peribronchiolar fibroblast population [4]. Importantly, a recent study identified similar *LGR5*$^+$ fibroblast populations in distal human airways [17]. Subclustering of this *Hhip*$^+$ peribronchiolar fibroblast population revealed additional complexity with *Lgr5/Lgr6* single- and double-positive populations (supplementary figure S1e–g). All cell types were lineage-labelled in the *Tcf21*m-Crem-R26R-tdTomato mouse, with exception of the *Hhip*$^+$ peribronchiolar fibroblasts (supplementary figure S1c and d). Thus, *Tcf21*lin$^-$ peribronchiolar fibroblasts may constitute a developmentally distinct lineage from *Tcf21*$^+$ stromal cells.

Next, we used targeted spatial transcriptomics [18] to multiplex the mRNA localisation of 18 cell type marker genes in six representative regions of adult murine lungs (n=2) along the proximal distal axis of the airway tree (figure 1d and supplementary figure S2a–c). *Hhip*$^+$/*Aspn*$^+$ peribronchiolar fibroblasts were enriched around airways, with some cells also in alveoli. *Myh11*$^+$/*Acta*$^+$ smooth muscle cells and *Serpinf1*$^+$/*Clec3b*$^+$ adventitial fibroblasts were enriched around airways and large vessels. *Gucy1a3*$^+$/*Postn*$^+$ pericytes localised preferentially to alveolar space and around larger vessels. The *Tcf21*hi/*Npnt*$^+$ lipofibroblasts were localised preferentially to alveolar space (figure 1e and supplementary figure S2d and e). Consequently, the number of cells in close physical proximity (direct cell–cell contact) to *Sftpc*$^+$ AT2 cells was highest for pericytes and lipofibroblasts with some *Hhip*$^+$/*Aspn*$^+$ cells also participating in the AT2 cell niche (figure 1f and supplementary figure S2f). Our data highlight the complexity of the AT2 cell niche, which we here demonstrate to contain at least three distinct stromal cell types.

An activated fibroblast state characterised by high Sfrp1 and Col28a1 expression

To follow the fate of fibroblasts during injury and repair we sorted cells from *Tcf21*m-Crem-R26R-tdTomato mice 14 days after bleomycin-induced lung injury (supplementary figures S1 and S3). Three injury-induced clusters became apparent (figure 2a and b), which were a mixture of *Tcf21*-lineage-positive and -negative cells. Interestingly, *Tcf21*-lineage-negative *Hhip*$^+$ peribronchiolar fibroblasts expanded (supplementary figure S1j, p and q), and some markers (*e.g. Lgr5* and *Lgr6*) were expressed in a myofibroblast subset (supplementary figure S1l), indicating that both *Tcf21*-lineage negative and positive cells converged into myofibroblasts.

We identified two *Cthrc1*$^+$/*Acta2*$^+$ myofibroblast types, with one subcluster showing enhanced *Spp1* expression (figure 2c and d). One cluster coexpressed myofibroblast genes with different fibroblast markers, especially from lipofibroblasts; hence, we named these “transitional fibroblasts” (figure 2b–d). Several genes, including the secreted frizzled-related protein 1 (*Sfrp1*), showed highest expression in this putative intermediate cell population (figure 2c and d; supplementary table S2). Gene–gene correlation of *Sfrp1* with other genes detected a transitional fibroblast core gene set, including *Col28a1* (supplementary figure S4d). Tissue proteomics revealed transient induction of COL28A1 and SFRP1 proteins after bleomycin injury (supplementary figure S4c) [19]. Co-staining SFRP1 and COL28A1 confirmed coexpression in ACTA2-low or -negative transitional cells (figure 2e), while CTHRC1$^+$ cells expressed higher levels of ACTA2 (figure 2f).

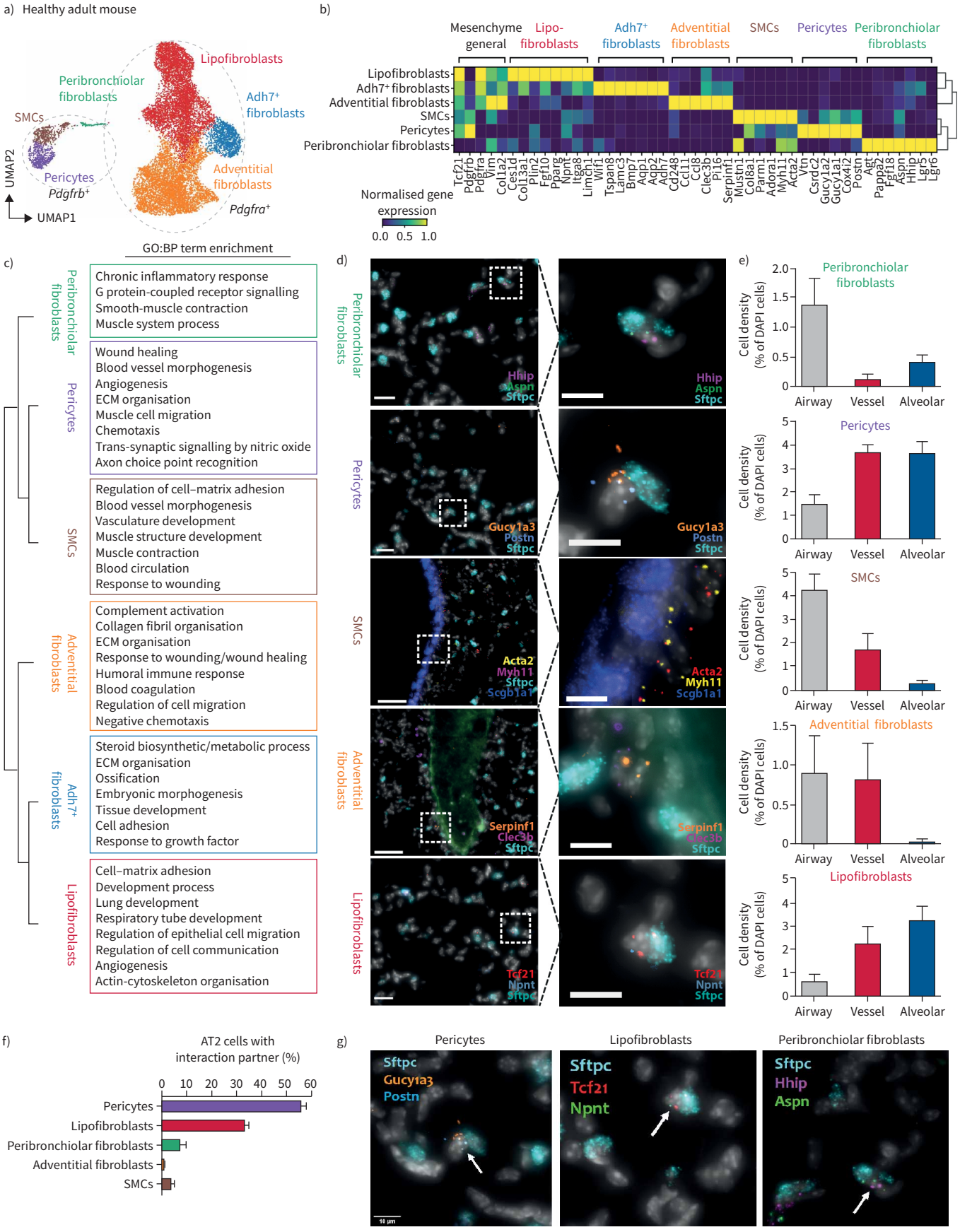
a) Healthy adult mouse
Lipofibroblasts
Peribronchiolar fibroblasts
Adh7+ fibroblasts
SMCs
Pericytes
Pdgfrb+
Adventitial fibroblasts
Pdgfra+
UMAP2
UMAP1
b)
Mesenchyme general
Lipo-fibroblasts
Adh7+ fibroblasts
Adventitial fibroblasts
SMCs
Pericytes
Peribronchiolar fibroblasts
Lipofibroblasts
Adh7+ fibroblasts
Adventitial fibroblasts
SMCs
Pericytes
Peribronchiolar fibroblasts
Tcf21 Pdgfrb Pdgfra Vim Col1a2 Ces1d Col13a1 Plin2 Fgf10 Pparg Npnt Itga8 Limch1 Wif1 Tspan8 Lamc3 Bmp7 Aqp1 Aqp2 Adh7 Cd248 Ccl11 Ccl8 Clec3b P16 Serpinf1 Mustn1 Col8a1 Parm1 Adora1 Myh11 Acta2 Vtn Csrdc2 Gucy1a2 Gucy1a1 Cox4i2 Postn Agt Pappa2 Fgf18 Aspn Hhip Lgr5 Lgr6
Normalised gene expression
0.0 0.5 1.0
c)
GO:BP term enrichment
Peribronchiolar fibroblasts
Chronic inflammatory response
G protein-coupled receptor signalling
Smooth-muscle contraction
Muscle system process
Pericytes
Wound healing
Blood vessel morphogenesis
Angiogenesis
ECM organisation
Muscle cell migration
Chemotaxis
Trans-synaptic signalling by nitric oxide
Axon choice point recognition
SMCs
Regulation of cell–matrix adhesion
Blood vessel morphogenesis
Vasculature development
Muscle structure development
Muscle contraction
Blood circulation
Response to wounding
Adventitial fibroblasts
Complement activation
Collagen fibril organisation
ECM organisation
Response to wounding/wound healing
Humoral immune response
Blood coagulation
Regulation of cell migration
Negative chemotaxis
Adh7+ fibroblasts
Steroid biosynthetic/metabolic process
ECM organisation
Ossification
Embryonic morphogenesis
Tissue development
Cell adhesion
Response to growth factor
Lipofibroblasts
Cell–matrix adhesion
Development process
Lung development
Respiratory tube development
Regulation of epithelial cell migration
Regulation of cell communication
Angiogenesis
Actin-cytoskeleton organisation
d)
Peribronchiolar fibroblasts
Hhip Aspn Sftpc
Pericytes
Gucy1a3 Postn Sftpc
SMCs
Acta2 Myh11 Sftpc Scgb1a1
Adventitial fibroblasts
Serpinf1 Clec3b Sftpc
Lipofibroblasts
Tcf21 Npnt Sftpc
e)
Peribronchiolar fibroblasts
Pericytes
SMCs
Adventitial fibroblasts
Lipofibroblasts
Cell density (% of DAPI cells)
Airway
Vessel
Alveolar
f)
AT2 cells with interaction partner (%)
0 10 20 30 40 50 60
Pericytes
Lipofibroblasts
Peribronchiolar fibroblasts
Adventitial fibroblasts
SMCs
g)
Pericytes
Sftpc Gucy1a3 Postn
Lipofibroblasts
Sftpc Tcf21 Npnt
Peribronchiolar fibroblasts
Sftpc Hhip Aspn

FIGURE 1 Stromal cell heterogeneity in the adult lung is associated with distinct spatial locations. a) Uniform manifold approximation and projection (UMAP) clustering depicts the seven distinct mesenchymal cell types (12 068 cells) identified in the healthy adult mouse lung. Circles mark *Pdgfra*- and *Pdgfrb*-expressing cells. b) The seven mesenchymal cell types are characterised with distinct gene expression profiles, as depicted in the matrixplot. c) Marker genes of the indicated mesenchymal subtypes are enriched for characteristic gene ontology (GO):biological process (BP) terms. False discovery rate <10%. Top 500 marker genes considered. d) Single mRNA multiplexed fluorescence *in situ* hybridisation (SCRINSHOT) with two cell type specific marker genes per cell type, as well as general markers allowed to identify preferential spatial locations of the mesenchymal cell types in the mouse lung. Scale bars=50 µm (overviews); 10 µm (insets). e) Localisation analysis shows stereotypic localisation of the mesenchymal cell types to peribronchiolar, adventitial and alveolar regions. The spatial location of 976 cells was quantified over five regions with 508 pericytes, 70 peribronchiolar cells, 206 lipofibroblasts, 41 adventitial fibroblasts and 151 smooth muscle cells (SMCs) counted. Graphs show cell density as percentage of cell type specific cells compared to all the cells (4′,6-diamidino-2-phenylindole (DAPI) stain-positive nuclei) in the area. Error bars represent SEM. f) Colocalisation analysis of 1269 alveolar type 2 (AT2) cells revealed preferred interaction partners among the mesenchymal cell types. A total of 291 AT2 interactions with mesenchymal cell types in the alveolar space were found: 167 pericytes; 93 lipofibroblasts, 15 peribronchiolar fibroblasts; three adventitial fibroblasts; 13 SMCs. g) SCRINSHOT pictures exemplifying the colocalisation of AT2 cells with distinct mesenchymal subtypes. Scale bars=10 µm. ECM: extracellular matrix.

To address clinical relevance, we compared *Col1a2*$^+$ cells after bleomycin injury with *COL1A2*$^+$ cells in ILD patients [20]. *SFRP1* was specific to *COL1A2*$^+$ mesenchymal cells and was weakly expressed in some *CLDN5*$^+$ endothelial cells (figure 2g). Expression was restricted to adventitial fibroblasts and disease enriched "inflammatory" fibroblast subsets (figure 2g and h). Increased expression of *SFRP1* in disease-induced fibroblast states was consistent in all three study cohorts (figure 2i and j). Importantly, in IPF tissues, more SFRP1$^+$ fibroblasts were present in mildly affected (early-stage) regions, while end-stage regions had more ACTA2$^+$ myofibroblasts localised to fibroblast foci (figure 2k–m). These data suggests a similar trajectory of fibroblast states in human lung fibrogenesis as seen in the bleomycin model.

Sfrp1$^+$ *transitional fibroblasts precede the appearance of* Cthrc1$^+$ *myofibroblasts*

To follow transcriptional dynamics of *Col1a2*$^+$ stromal cells during inflammatory, fibrogenic and resolution phases of lung regeneration, we collected *Epcam*$^-$/*Pecam1*$^-$/*Lyve1*$^-$/*CD45*$^-$ stromal cells at 18 time points after bleomycin injury (figure 3a–c). This longitudinal scRNAseq dataset of *Col1a2*$^+$ cells (69 185 cells) (figure 3b) featured three distinct injury-induced cell states (supplementary figure S4a) similar to the *Tcf21*-lineage tracing dataset (figure 3c and supplementary table S3). *Sfrp1*$^+$ transitional fibroblasts peaked at day 3, preceding *Spp1*$^+$ and *Cthrc1*$^+$ myofibroblasts at day 9 to day 21 (figure 3d). Proliferation analysis showed a transient increase in proliferation rates, mainly in Spp*1*$^+$ and *Cthrc1*$^+$ myofibroblasts, returning to baseline from day 28 onwards (supplementary figure S4b). This suggests the early post-injury increase of *Sfrp1*$^+$ cells was not from expanding pre-existing cells, but from differentiating baseline fibroblast states. Using immunofluorescence (figure 3e–l), we found that in healthy lungs, signals for

FIGURE 2 Three distinct activated mesenchymal cell types emerge after bleomycin (bleo)-induced mouse lung injury. a) Uniform manifold approximation and projection (UMAP) depicts mesenchymal cell types (n=12 254 cells) identified at day 14 (d14) after bleomycin injury. b) The marker genes of activated mesenchymal subtypes are enriched for characteristic gene ontology (GO):biological process (BP) terms. False discovery rate <10%. Top 500 marker genes considered. c) The dotplot depicts a gradient of marker gene expression across the activated cell types. d) The mesenchymal cell types are characterised with distinct gene expression profiles, as depicted in the matrixplot. e, f) Immunofluorescence analysis of lung tissue sections from bleomycin-treated mice demonstrates colocalisation of SFRP1 (red) and COL28A1 (green) 14 days after injury. Arrowheads in the magnified insets indicate SFRP1/COL28A1 double-positive cells. SFRP1/COL28A1 double-positive cells did not colocalise with α-smooth muscle actin (ACTA)2 (cyan). No expression of SFRP1 was detected in PBS controls. Scale bars=100 µm (PBS), 100 µm (Bleo d14) and 50 µm (inset). f) At d14 after injury, ACTA2 (green) and CTHRC1 (red) double-positive cells were found (indicated by arrowheads in the magnified insets for ROI1 and ROI2 in the very right panel). Nuclei in blue colour (4′,6-diamidino-2-phenylindole DAPI). Scale bars=100 µm and 20 µm (inset). g, j) Distinct markers from the bleomycin mouse model were analysed in a recently published integrated atlas of human lung fibrosis at single-cell resolution [20]. g) *SFRP1* showed specific expression on human *COL1A2*$^+$ positive mesenchymal cells. h) Marker gene expression across all mesenchymal cell types identified in the human lung. i, j) Differential gene expression analysis between interstitial lung disease (ILD) patient samples and healthy control samples: i) reveals significant regulation of *SFRP1* in adventitial fibroblasts (AdvF) and inflammatory fibroblasts cluster 2; j) this regulation is consistent across all three cohorts in the atlas. k) Immunofluorescence analysis of micro-CT staged idiopathic pulmonary fibrosis (IPF)-patient tissues demonstrating an increase of SFRP1 (red) in regions of mild fibrosis (IPF stage I) compared to healthy controls. In regions of severe fibrosis (IPF stage III) and tissue remodelling, fibroblastic foci (white dashed lines, FF) stained positive for α-smooth muscle actin (ACTA2) (green), but mostly not for SFRP1. Adjacent to fibroblastic foci (A-FF) SFRP1 expressing fibroblasts were still present. Scale bars=200 µm. Representative images are shown. l) Quantification of SFRP1's mean fluorescence intensity (MFI) of various regions-of-interest (ROIs) from three different patients (n=3). Statistics: one-way ANOVA. m) Quantification of SFRP1 MFI in late-stage IPF comparing SFRP1 expression within fibroblastic foci (FF) and adjacent to fibroblastic foci (A-FF) from three different patients (n=3). Statistics: unpaired t-test. ****: p<0.0001. SMC: smooth muscle cell; ECM: extracellular matrix.

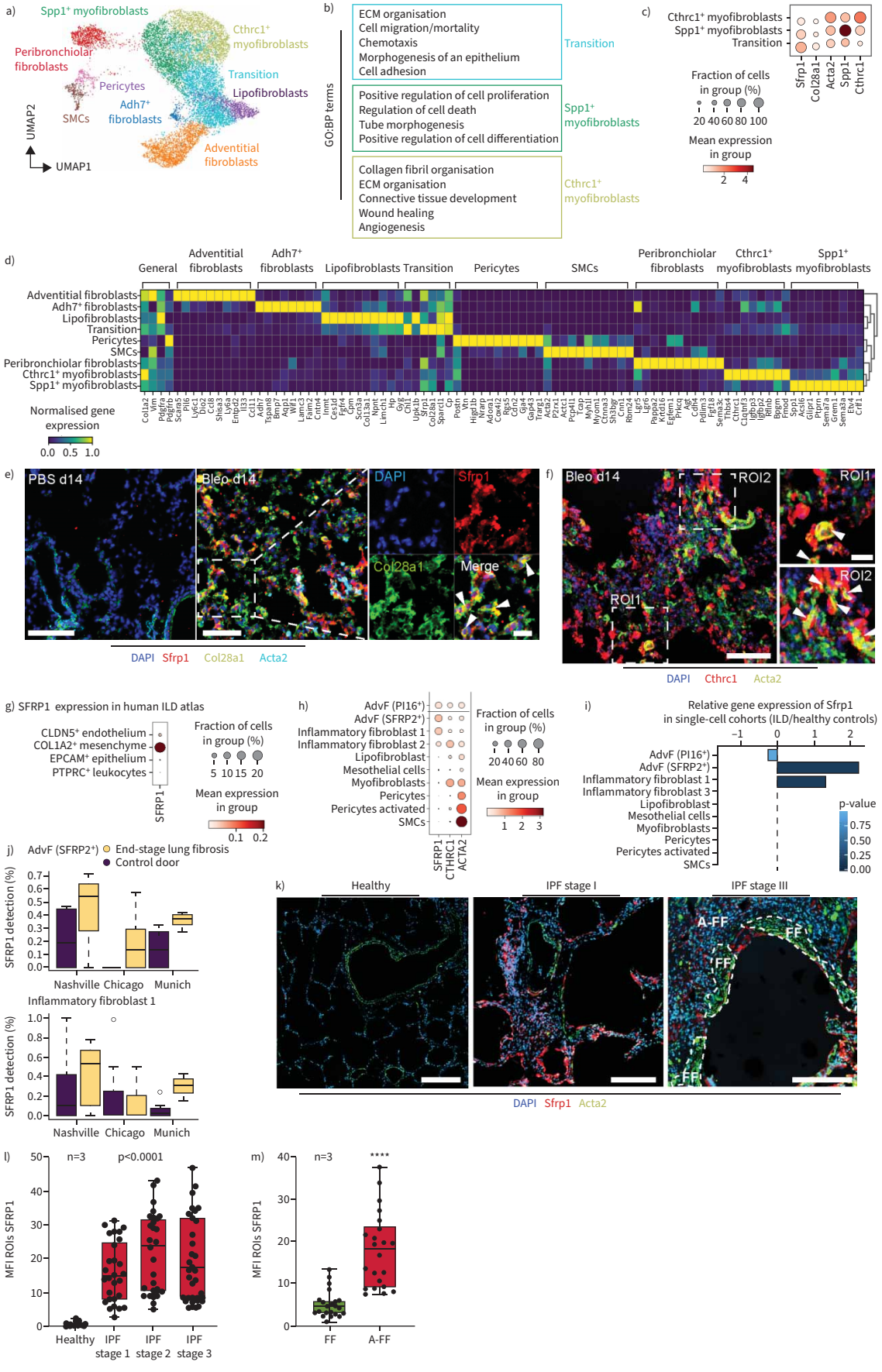
a)
Spp1+ myofibroblasts
Cthrc1+ myofibroblasts
Peribronchiolar fibroblasts
Transition
Pericytes
Lipofibroblasts
Adh7+ fibroblasts
SMCs
Adventitial fibroblasts
UMAP2
UMAP1
b)
GO:BP terms
ECM organisation
Cell migration/mortality
Chemotaxis
Morphogenesis of an epithelium
Cell adhesion
Transition
Positive regulation of cell proliferation
Regulation of cell death
Tube morphogenesis
Positive regulation of cell differentiation
Spp1+ myofibroblasts
Collagen fibril organisation
ECM organisation
Connective tissue development
Wound healing
Angiogenesis
Cthrc1+ myofibroblasts
c)
Cthrc1+ myofibroblasts
Spp1+ myofibroblasts
Transition
Sfrp1
Col28a1
Acta2
Spp1
Cthrc1
Fraction of cells in group (%)
20 40 60 80 100
Mean expression in group
2 4
d)
General
Adventitial fibroblasts
Adh7+ fibroblasts
Lipofibroblasts
Transition
Pericytes
SMCs
Peribronchiolar fibroblasts
Cthrc1+ myofibroblasts
Spp1+ myofibroblasts
Adventitial fibroblasts
Adh7+ fibroblasts
Lipofibroblasts
Transition
Pericytes
SMCs
Peribronchiolar fibroblasts
Cthrc1+ myofibroblasts
Spp1+ myofibroblasts
Normalised gene expression
0.0 0.5 1.0
e)
PBS d14
Bleo d14
DAPI
Sfrp1
Col28a1
Merge
DAPI Sfrp1 Col28a1 Acta2
f)
Bleo d14
ROI1
ROI2
DAPI Cthrc1 Acta2
g) SFRP1 expression in human ILD atlas
CLDN5+ endothelium
COL1A2+ mesenchyme
EPCAM+ epithelium
PTPRC+ leukocytes
SFRP1
Fraction of cells in group (%)
5 10 15 20
Mean expression in group
0.1 0.2
h)
AdvF (PI16+)
AdvF (SFRP2+)
Inflammatory fibroblast 1
Inflammatory fibroblast 2
Lipofibroblast
Mesothelial cells
Myofibroblasts
Pericytes
Pericytes activated
SMCs
SFRP1
CTHRC1
ACTA2
Fraction of cells in group (%)
20 40 60 80
Mean expression in group
1 2 3
i)
Relative gene expression of Sfrp1 in single-cell cohorts (ILD/healthy controls)
−1 0 1 2
AdvF (PI16+)
AdvF (SFRP2+)
Inflammatory fibroblast 1
Inflammatory fibroblast 3
Lipofibroblast
Mesothelial cells
Myofibroblasts
Pericytes
Pericytes activated
SMCs
p-value
0.75
0.50
0.25
0.00
j)
AdvF (SFRP2+)
End-stage lung fibrosis
Control door
SFRP1 detection (%)
Nashville Chicago Munich
Inflammatory fibroblast 1
SFRP1 detection (%)
Nashville Chicago Munich
k)
Healthy
IPF stage I
IPF stage III
A-FF
FF
FF
FF
DAPI Sfrp1 Acta2
l)
n=3
p<0.0001
MFI ROIs SFRP1
Healthy
IPF stage 1
IPF stage 2
IPF stage 3
m)
n=3
****
MFI ROIs SFRP1
FF
A-FF

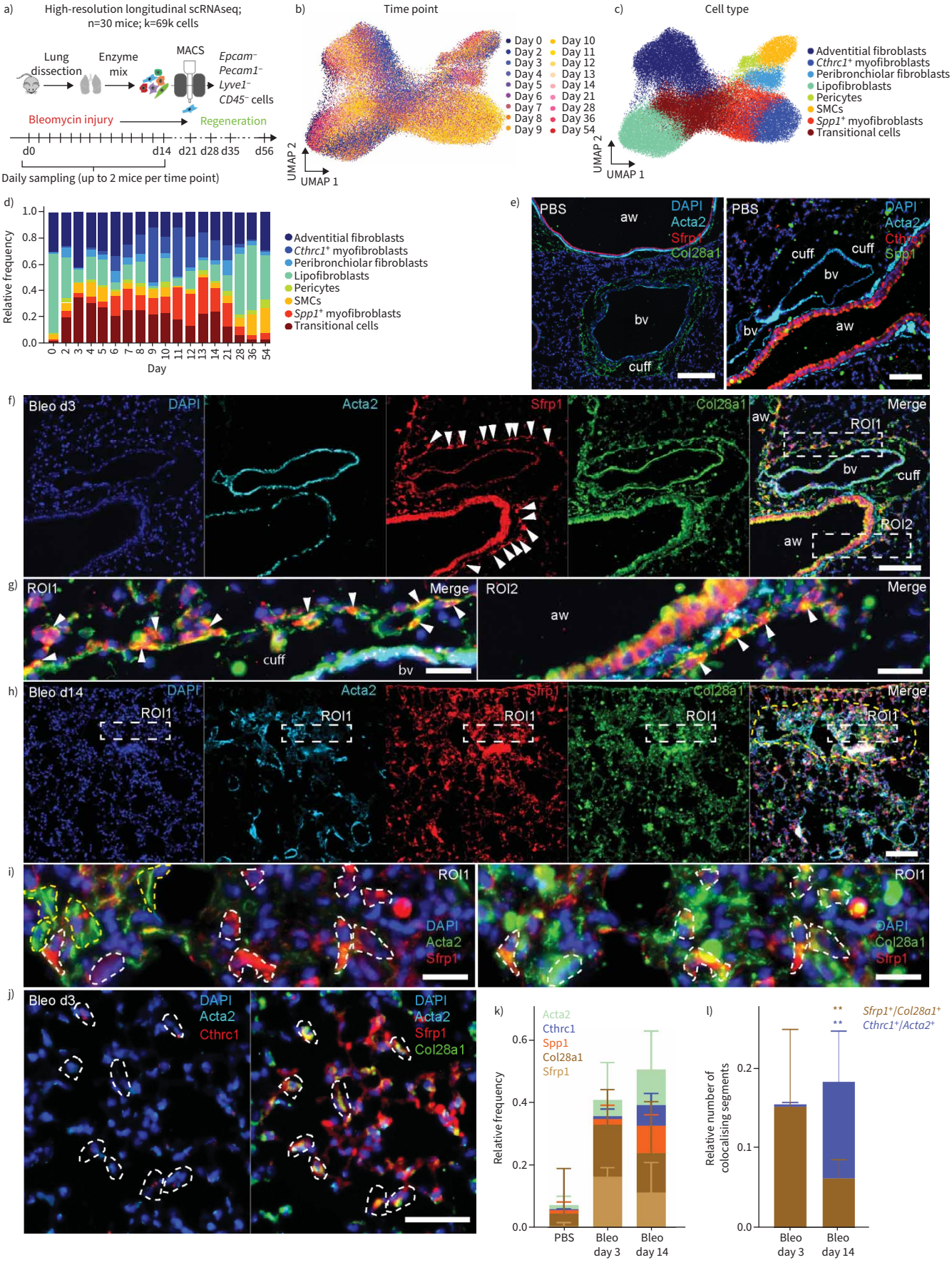
a)
High-resolution longitudinal scRNAseq;
n=30 mice; k=69k cells
Lung dissection
Enzyme mix
MACS
Epcam⁻ Pecam1⁻ Lyve1⁻ CD45⁻ cells
Bleomycin injury
Regeneration
d0 d14 d21 d28 d35 d56
Daily sampling (up to 2 mice per time point)
b)
Time point
Day 0 Day 2 Day 3 Day 4 Day 5 Day 6 Day 7 Day 8 Day 9 Day 10 Day 11 Day 12 Day 13 Day 14 Day 21 Day 28 Day 36 Day 54
UMAP 1
UMAP 2
c)
Cell type
Adventitial fibroblasts
Cthrc1+ myofibroblasts
Peribronchiolar fibroblasts
Lipofibroblasts
Pericytes
SMCs
Spp1+ myofibroblasts
Transitional cells
d)
Relative frequency
Day
e)
PBS
aw
bv
cuff
DAPI
Acta2
Sfrp1
Col28a1
Cthrc1
Spp1
f)
Bleo d3
Merge
ROI1
ROI2
g)
h)
Bleo d14
i)
j)
k)
Relative frequency
PBS
Bleo day 3
Bleo day 14
l)
Relative number of colocalising segments
Sfrp1+/Col28a1+
Cthrc1+/Acta2+

FIGURE 3 *Sfrp1*$^+$ transitional fibroblasts emerge in adventitial and alveolar space upon injury preceding the emergence of *Cthrc1*$^+$ myofibroblasts. a) A high-resolution longitudinal dataset was generated by subjecting magnetic-activated cell-sorting (MACS)-sorted cells from the mesenchymal compartment to single-cell RNA-sequencing (scRNAseq) at the 18 indicated time points. Uniform manifold approximation and projection (UMAP) embedding displays cells coloured by b) time point and c) cell type identity. d) The distribution of cell type frequencies across time points. e) Immunofluorescence analysis of lung tissue sections from PBS control mice. In the left panel, cell nuclei were immunostained with 4′,6-diamidino-2-phenylindole DAPI (blue) and smooth muscle cells (SMCs) with α-smooth muscle actin (ACTA)2 (cyan). SFRP1 (red) staining was absent apart from nonspecific signals in bronchial epithelial cells. COL28A1 (green) was mostly found as a filamentous staining in "cuffs" surrounding blood vessels (bv). In the right panel, cell nuclei were stained with DAPI (blue) and SMCs with ACTA2 (cyan). CTHRC1 (red) staining was absent apart from nonspecific signals in bronchial epithelial cells. SPP1 is depicted in green. Scale bars=100 µm. f) Immunofluorescence analysis of lung tissue sections from bleomycin-treated mice at day 3 after injury (Bleo d3) demonstrating appearance of SFRP1 (red) positive cells surrounding blood vessels and airways (aw) (arrowheads). Scale bar=100 µm. g) Arrowheads in the magnified insets taken from region of interest (ROI)1 and ROI2 of figure 4f indicate SFRP1/COL28A1 double-positive cells surrounding blood vessels in ROI1 reminiscent of adventitial fibroblasts, as well as surrounding airways (aw) in ROI2 reminiscent of peribronchiolar fibroblasts. Scale bars=20 µm. h) Yellow dashed line indicates a fibrotic region of lung tissue after 14 days of bleomycin treatment. ACTA2 staining in cyan exhibits the appearance of myofibroblasts, and concomitant expression of SFRP1 (red) and COL28A1 (green) in this fibrotic region. Cell nuclei are stained with DAPI in blue. Scale bar=100 µm. A magnified view of fibrotic ROI1 is displayed in (i), in the left panel demonstrating mutually exclusive appearance of SFRP1$^+$ (red and dashed white lines) and ACTA2$^+$ (green and dashed yellow lines) cells. Here, for better detection of colocalisation signals between ACTA2 and SFRP1, we switched colours of ACTA2 from cyan as depicted in (h) to green. The right panel denotes SFRP1 (red) and COL28A1 (green) double-positive cells encircled with white dashed lines. Cell nuclei stained with DAPI in blue. Scale bars=20 µm. j) Iterative immunofluorescence staining of parenchymal lung tissue (4i-FFPE) at day 3 after injury indicating COL28A1 (green)/SFRP1 (red) double-positive cells in the left image. The same cells, as indicated by white dashed lines, were found to be CTHRC1- (red) and ACTA2- (cyan) negative. Scale bar=50 µm. A larger overview image can be found in supplementary figure S7a. k) Stacked bar-plot denoting relative frequencies of ACTA2-, CTHRC1-, SPP1-, COL28A1- and SFRP1-positive tissue segments at day 3 and day 14 after bleomycin treatment and compared to PBS controls from software-based segmented images as exemplified in supplementary figure S7c. Three different ROIs (each 1.1 mm^2 in size) from two different mice for each condition were analysed. l) Quantification of double-positive SFRP1$^+$/COL28A1$^+$ and CTHRC1$^+$/ACTA2$^+$ tissue segments were analysed by fluorescent-signal colocalisation (supplementary figure S7d), its segmentation and software-based quantification. The number of colocalising tissue segments relative to the total cell count (20 691 cells) is shown. 10–20 different 0.1–0.25-mm^2 ROIs (peribronchial/perivascular/parenchymal on day 3 compared to fibrotic on day 14) from two different mice per condition were analysed. Statistics: two-way ANOVA with Tukey's multiple comparison: **: p<0.01.

SFRP1, CTHRC1 and SPP1 were mostly absent, except for nonspecific signals in the airway epithelium's luminal areas (figure 3e). Filamentous COL28A1 localised around bronchovascular cuffs, whereas ACTA2 was primarily observed in smooth muscle cells near airways and blood vessels (figure 3e). Localisation of adventitial and peribronchial fibroblasts next to bronchovascular cuffs has been described [1] and concurs with our single-molecule fluorescence *in situ* hybridisation (smFISH) analysis (figure 1).

3 days post-injury, SFRP1/COL28A1 double-positive cells emerged around airways, blood vessels and alveoli, with ACTA2 expressed in bronchovascular smooth muscle cells (figure 3f, g and j). In contrast, at day 14 post-injury, ACTA2-myofibroblasts and SFRP1$^+$/COL28A1$^+$ cells coexisted in fibrotic dense areas (figure 3h and i). Multiplexed immunofluorescence-analysis confirmed the increase of SFRP1$^+$/COL28A1$^+$ transitional cells at day 3, and until day 14 post-injury expanding SPP1$^+$ and CTHRC1$^+$ myofibroblasts (figure 3k and l; total analysis of 20 691 cells, supplementary figure S7c), thus verifying our data in figure 3d on protein level.

Convergence of multiple mesenchymal cell types towards myofibroblast identity

To infer lineage relationships between the different cell types and activation states we used CellRank (figure 4) [21]. We analysed three phases as "early injury" (figure 4a–c), "fibrogenesis" (figure 4d–f) and "resolution" (figure 4g–i). CellRank computed fate probabilities for each cell, showing their specific differentiation potential towards a "terminal state" end-point in the time-course data. Heatmaps demonstrate fate probability (figure 4a, d and g), and violin plots visualise the probability distribution among the cells for

FIGURE 4 Lineage convergence and two-way conversion of fibroblasts in lung regeneration. a, d, g) CellRank's coarse-grained and directed transition matrix was calculated for the given three phases of the bleomycin lung injury time course, of early phase (day 2 to day 5), fibrogenesis phase (day 6 to day 21) and resolution phase (day 28 to day 54). Terminal macrostates were set manually and annotated according to their overlap with the underlying gene expression clusters. The heatmap represents the mean absorption probabilities of every cell in the given cell types to the terminal fates. b, e, h) Violin plots indicating the absorption probability towards the specified fate for every cell in all the cell types. c, f, i) Scatter plots show top driver genes, predicted to facilitate transition to the given terminal fate, visualised as gene-correlations between two terminal fate lineages. The top genes of a third lineage are visible by the third colour of the gene names. Dots are coloured according to their mean gene expression. SMC: smooth muscle cell.

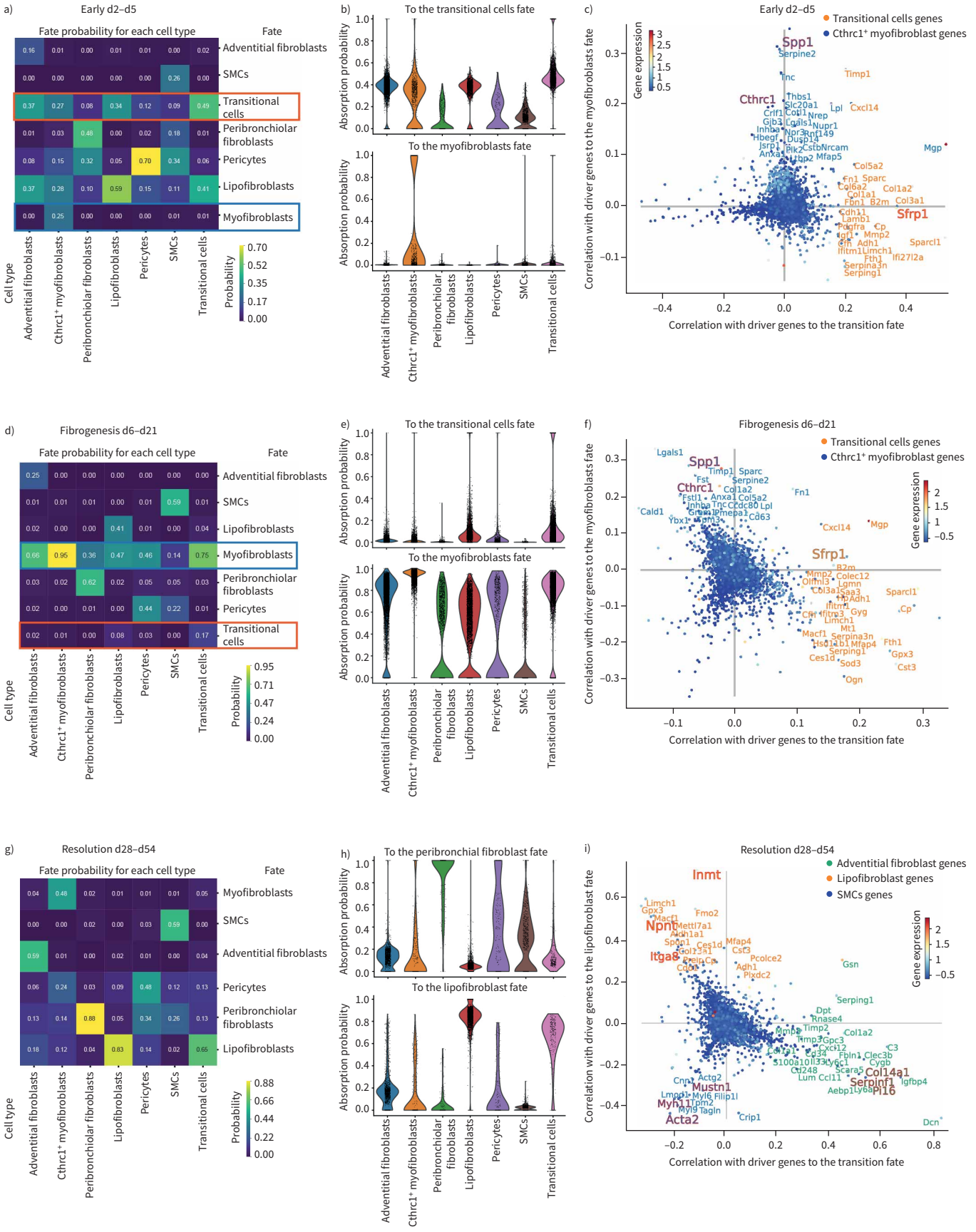
a)
Early d2–d5
Fate probability for each cell type
Fate
Adventitial fibroblasts
SMCs
Transitional cells
Peribronchiolar fibroblasts
Lipofibroblasts
Pericytes
Myofibroblasts
Cell type
Probability
b)
To the transitional cells fate
To the myofibroblasts fate
Absorption probability
c)
Early d2–d5
Transitional cells genes
Cthrc1+ myofibroblast genes
Gene expression
Correlation with driver genes to the myofibroblasts fate
Correlation with driver genes to the transition fate
d)
Fibrogenesis d6–d21
e)
f)
g)
Resolution d28–d54
h)
To the peribronchial fibroblast fate
To the lipofibroblast fate
i)
Adventitial fibroblast genes
Lipofibroblast genes
SMCs genes
Correlation with driver genes to the lipofibroblast fate

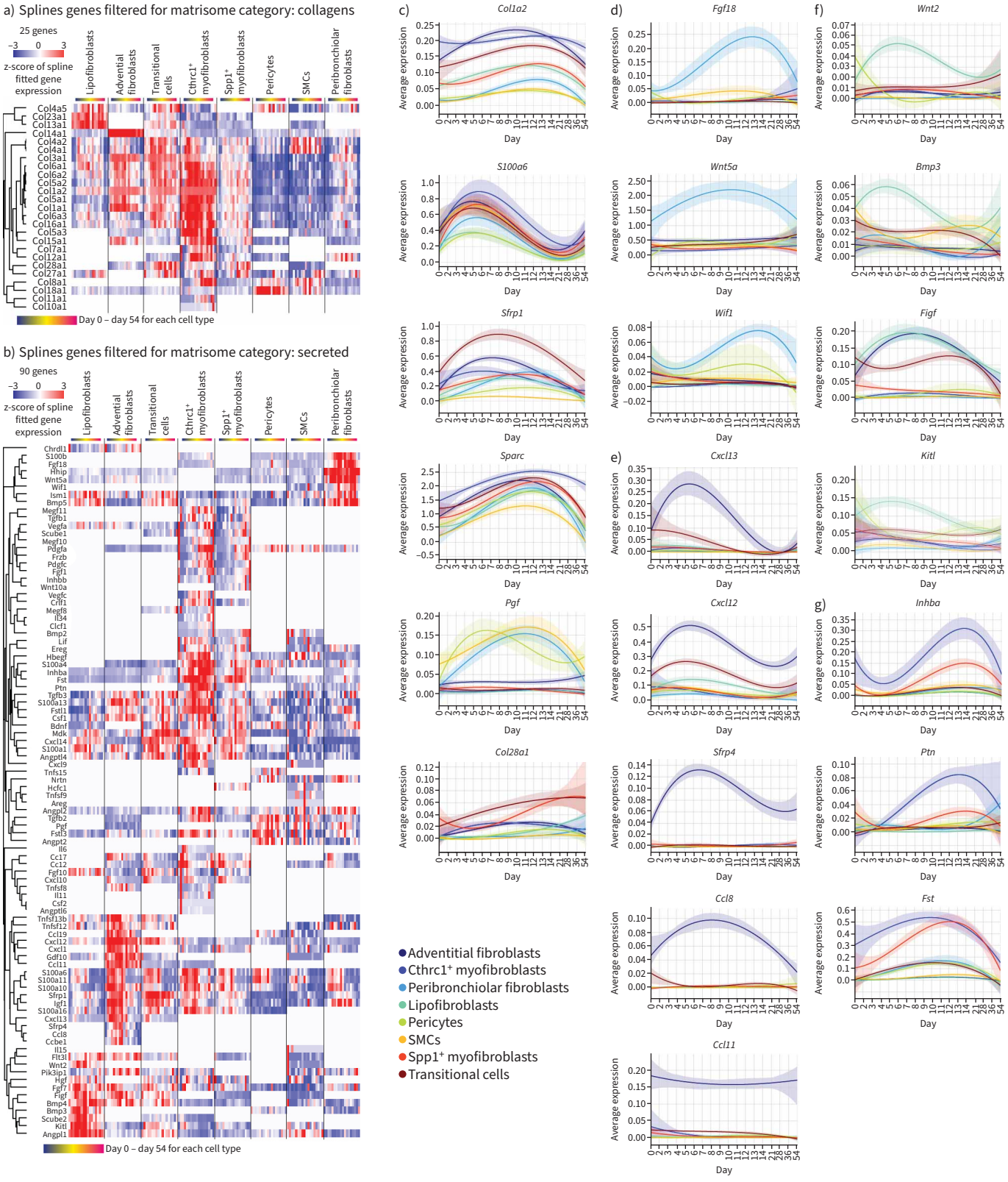

FIGURE 5 Highly specific expression changes in distinct fibroblast lineages. a, b) Heatmaps display genes that showed differential expression along the time-course in at least one cell type using a spline regression model for a) 25 different collagens and b) 90 secreted matrisome [22] genes. c–g) Line plots show average expression of indicated genes for each cell type along the bleomycin time course, for c) general mesenchymal marker genes, d) genes regulated over time in peribronchial fibroblasts, e) adventitial fibroblast, f) lipofibroblasts and g) *Cthrc1*$^{+}$ myofibroblasts. SMC: smooth muscle cell.

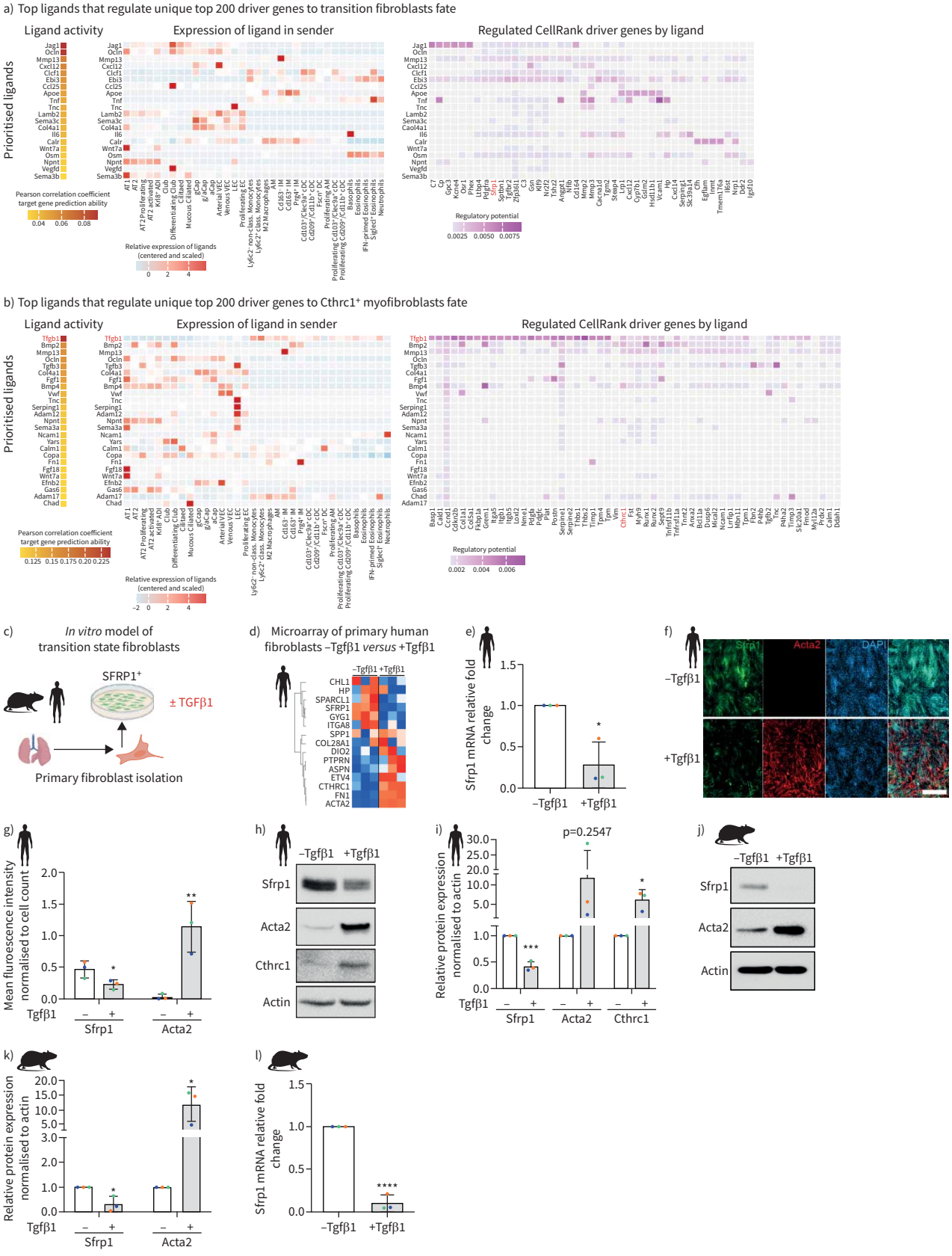

FIGURE 6 *Tgfβ1* drives conversion of *Sfrp1*$^{+}$ transitional cells to *Cthrc1*$^{+}$ myofibroblasts. a, b) NicheNet analysis based prediction of regulatory ligands upstream of fibroblast states. Heatmaps show top ranked ligands with highest potential of regulating the top 200 driver genes towards the

fate of a) *Sfrp1*$^+$ transitional fibroblasts and b) *Cthrc1*$^+$ myofibroblasts. The left panel shows scaled expression of those ligands across cell types of the whole lung, while the right panel shows the top downstream target genes of each ligand. c) Experimental design. d) Heatmap shows z-scored gene expression from bulk transcriptomics after transforming growth factor (TGF)β1 treatment of primary human fibroblasts grown *in vitro*. e) mRNA (quantitative (q)PCR) expression of *SFRP1* 48 h after TGFβ1-treatment of primary human lung fibroblasts grown *in vitro*. f) Immunofluorescence staining and g) quantification thereof of primary human lung fibroblasts showing the expression of SFRP1 and ACTA2 with and without 48 h of TGFβ1-treatment. Scale bar=250 µm. h) Protein expression of SFRP1, ACTA2 and CTHRC1 by Western blotting and i) its quantification using human lung fibroblasts cultured *in vitro* for 48 h with and without TGFβ1. Representative of n=3. j) Protein expression of SFRP1 and ACTA2 by Western blotting and k) its quantification using mouse lung fibroblasts cultured *in vitro* for 48 h with and without TGFβ1. Representative of n=3. l) mRNA (qPCR) expression of *Sfrp1* 48 h after TGFβ1-treatment of primary mouse lung fibroblasts grown *in vitro*. All data are shown as mean±SD with n=3 from different mice or human donors. *: p<0.05, **: p<0.01, ***: p<0.001, ****: p<0.0001 by unpaired two-tailed t-tests.

selected fates in each cell type (figure 4b, e and h). Key lineage driver genes correlating with different fate trajectories are depicted in scatter plots (figure 4c, f and i). Early injury phase analysis (days 2–5) showed that adventitial fibroblasts and lipofibroblasts had a high fate probability of transitioning to the *Sfrp1*$^+$ state (figure 4a and b). Probabilities towards myofibroblasts were low, represented only by few *Cthrc1*$^+$ myofibroblasts (figure 4a and b). Top driver genes towards transitional cells included various collagens, chemokines and notably *Sfrp*1, while the myofibroblast lineage showed marker genes including *Tnc*, *Spp1* and *Thbs1* (figure 4c). In the fibrogenesis phase (day 6 to day 21), fate probabilities predicted *Sfrp1*$^+$ cells transitioning to myofibroblasts (figure 4d,e). Top driver genes towards myofibroblasts represented classical myofibroblast-associated genes including *Lgals1*, *Sparc* and *Spp1* as well as *Cthrc1* (figure 4f). In the resolution phase, differentiation probabilities suggested a reversion of *Cthrc1*$^+$ myofibroblasts towards lipofibroblast, peribronchiolar fibroblast and pericyte states (figure 4g and i). This prediction correlates with previous observations of a two-way conversion between lipogenic and myogenic fibroblastic phenotypes [6].

Next, we used a spline regression model revealing genes with differential expression in at least one cell type over time (supplementary table S4). We found 25 different collagens with dynamic expression patterns after injury or between various stromal cells (figure 5a). Additionally, 90 secreted matrisome [22] genes with significant expression changes along the injury time-course were identified (figure 5b). All cell types displayed transiently increased expression of collagen type-I (*Col1a2*) and the ECM protein Sparc, a marker for myofibroblasts (figure 5c) [23]. We also observed common early fibroblast activation events, like the early post-injury upregulation of *S100a6* (figure 5c). Peribronchiolar fibroblasts specifically featured important secreted morphogens like *Hhip*, *Wif1*, *Fgf18* and *Wnt5a* (figure 5d). This matters as fibroblast-derived Wnt-signaling, especially *Wnt5a*, defines a specific AT2 cell niche in normal homeostasis [24], is part of a distinct mesenchymal niche in human distal airways, and is secreted by LGR5$^+$ fibroblasts [17]. Adventitial fibroblasts specifically produced the Wnt modulator *Sfrp4*, besides injury-induced chemokines like *Cxcl13* for B-cell recruitment, and *Cxcl12* and *Ccl8* to attract T-cells, monocytes and neutrophils. Interestingly, the chemokine eotaxin (*Ccl11*) specifically marked adventitial fibroblasts, unaffected by injury (figure 5e). Lipofibroblasts specifically expressed the morphogens *Wnt2* and *Bmp3*, plus stem cell factor (SCF) (*Kitl*) (figure 5f). The SCF-c-Kit pathway is activated in bleomycin-injured lungs, with potential profibrotic effects *via* recruitment of Kit$^+$ immune cells to the lung [25].

Conclusively, our data suggest that early after injury multiple mesenchymal cell types converge towards *Sfrp1*$^+$ transitional cells, which ultimately give rise to *Cthrc1*$^+$ myofibroblasts, with a potential to revert towards lipofibroblasts, peribronchiolar fibroblasts and pericytes during the resolution phase.

TGFβ mediates differentiation of Sfrp1$^+$ *transitional fibroblasts into myofibroblasts*

To infer potential regulators of the fibroblast cell state transitions after injury we used NicheNet [26], which predicted the ligands with highest probability to induce expression of the top driver genes from the CellRank outputs (figure 4) for *Sfrp1*$^+$ transitional cells and *Cthrc1*$^+$ myofibroblasts (figure 6a and b). The top ligand upstream of *Sfrp1*$^+$ transitional cells was the Notch ligand *Jag1*, predominantly expressed in secretory airway epithelial cells, and to a lesser degree in alveolar epithelial and vascular endothelial cells (figure 6a). Consistent with our finding here, Notch deficiency in mesenchymal cells reportedly reduced fibrotic remodelling and myofibroblast differentiation in the bleomycin model [27]. Notably, upstream of *Sfrp1*$^+$ transitional cell state driver genes the top ligands excluded Tgfβ, which was the top ranked ligand for *Cthrc1*$^+$ myofibroblast driver genes. *Tgfβ1* was the top ligand, primarily expressed by myeloid lineage immune cells, along with *Tgfβ3* expressed by activated AT2 cells and lymphatic endothelial cells (figure 6b).

Culturing isolated primary mouse and human lung fibroblasts *in vitro*, we observed marker gene expression consistent with the *in vivo Sfrp1*$^+$ transitional state (figure 6c and d). Myofibroblast identifiers like CTHRC1

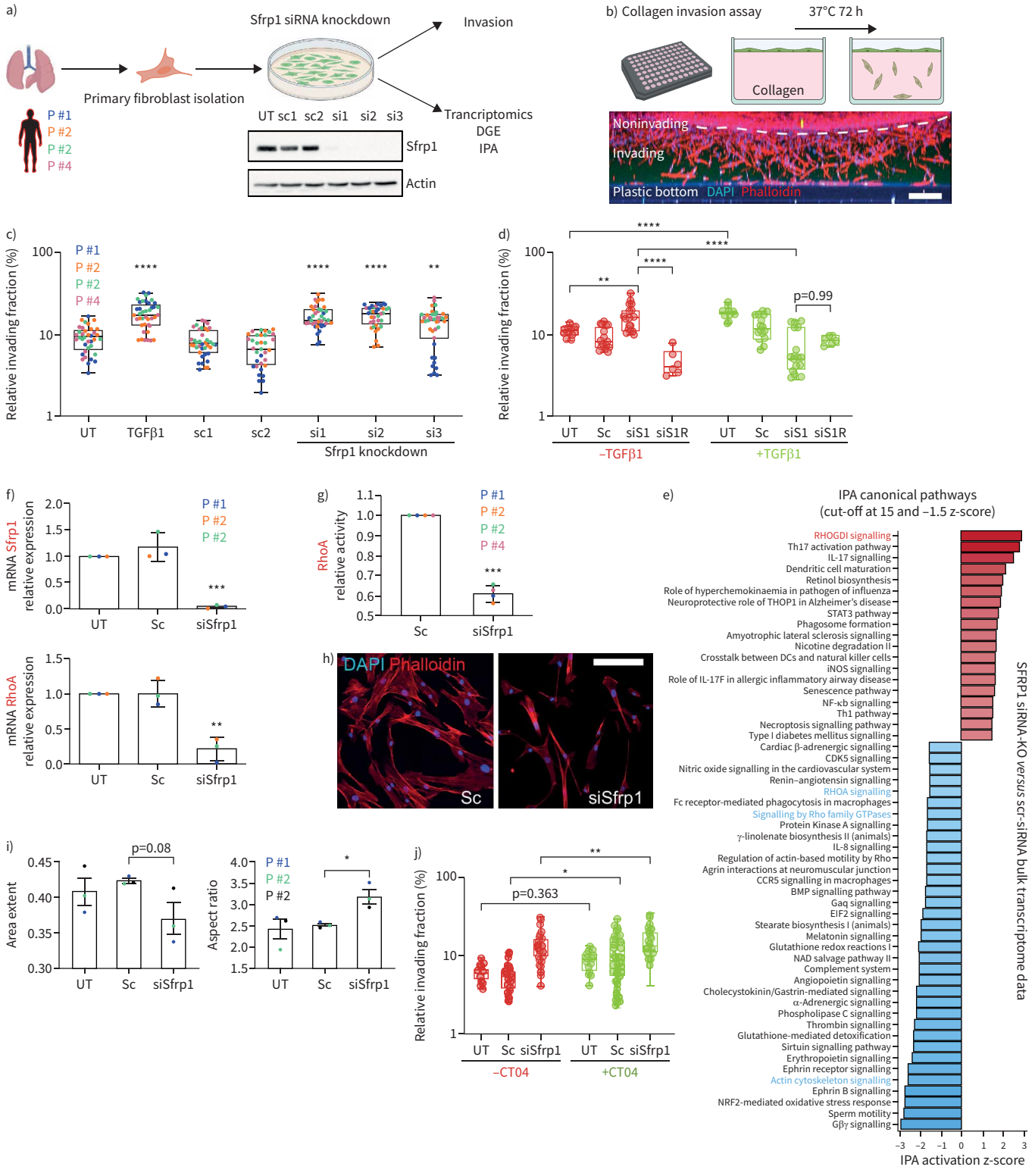

FIGURE 7 SFRP1 in transition state fibroblasts regulates invasion, RHOA activity and cell shape. a) Primary human fibroblasts were isolated from lungs of human patients and cultured on rigid two-dimensional surfaces. SFRP1 expression was diminished in these cells by application of three different siRNAs targeting various exons. The successful knockdown of SFRP1 protein was confirmed by Western blot analysis. b) Primary human fibroblasts were applied on top of a collagen extracellular matrix (ECM) and left to invade for 72–96 h. Cells were stained for nuclei (4′,6-diamidino-2-phenylindole (DAPI), blue) and filamentous actin (phalloidin, red). A maximum intensity projection of a z-stack from one entire well is depicted as xz-view. Scale bar=200 µm. c) Transforming growth factor (TGF)β1-treatment as well as SFRP1-depletion augmented the ECM invasion capacity of primary human lung fibroblasts. Data are presented as mean±SD. One-way ANOVA with Tukey's multiple comparison test, n=4

(fibroblasts from four different patients displayed as distinct colours). Logarithmic (log_{10}) y-axis. d) Addition of recombinant SFRP1 (R) rescued the increased invasion of SFRP1-depleted human lung fibroblasts (siS1R^{-}TGFβ1) as well as partially the reduced invasion of TGFβ1-treated and SFRP1-depleted fibroblasts (siS1R^{+}TGFβ1). Sc shows pooled data from Sc1-2. SiRNA shows pooled data from siRNA1-3. One-way ANOVA with Tukey's multiple comparison test, n=1–3 (fibroblasts from up to three different patients). Logarithmic (log_{10}) y-axis. e) Ingenuity pathway analysis (IPA) canonical pathway analysis based on bulk transcriptome data analysis of SFRP1-siRNA-depleted compared to SFRP1-expressing primary human lung fibroblasts. IPA identified RHOA-signalling as a highly affected pathway in SFRP1-siRNA-depleted fibroblasts. f) Transcript analysis by quantitative PCR confirmed the successful reduction of Sfrp1 mRNA in Sfrp1-siRNA-treated primary human lung fibroblasts. RHOA mRNA was found to be considerably reduced in SFRP1-depleted fibroblasts. Data are presented as mean±SD. Unpaired two-tailed t-test. n=3 (fibroblasts from three different patients). g) Consistent with IPA analysis shown in (e) as well as reduction of RHOA mRNA displayed in (f), RHOA-GTPase activity was significantly reduced in SFRP1-depleted primary human lung fibroblasts. Data are presented as mean±SD. Unpaired two-tailed t-test. n=4 (fibroblasts from four different patients). h) Immunofluorescence labelling of filamentous actin cytoskeleton (phalloidin in red) indicated a morphological switch towards smaller and elongated cell shapes in SFRP1-depleted primary human lung fibroblasts. Scale bar=100 µm. i) Detailed cell morphological analysis using an automatised workflow in CellProfiler software. The unbiased quantification of 1000 cells from untreated (UT), scrambled-siRNA-treated (Sc) and SFRP1-siRNA-treated (siSfrp1) human lung fibroblasts confirmed a substantial switch towards more elongated (smaller area extent, higher aspect ratio) cell morphologies in SFRP1-depleted primary human lung fibroblasts. In total we analysed up to 15 000 single cells from each condition and patient. Data are presented as mean±SD. Unpaired t-test. p=0.08, n=3 (fibroblasts from three different patients). j) RHOA-GTPase inhibition by CT04 (C3 transferase) triggered an increase in the invasive capacity of primary human lung fibroblasts. Sc shows pooled data from Sc1-2. SiRNA shows pooled data from siRNA1-3. One-way ANOVA with Tukey's multiple comparison test, n=4 (fibroblasts from four different patients). Logarithmic (log_{10}) y-axis. *: p<0.05, **: p<0.01, ***: p<0.001, ****: p<0.0001.

and SPP1, and fibrosis-relevant ECM marker FN1, were upregulated upon TGFβ1 stimulation, while SFRP1 was downregulated (figure 6d). We validated these observations in human and mouse primary lung fibroblasts using quantitative PCR (figure 6e and l), immunofluorescence (figure 6f and g) and Western blotting (figure 6i–k). Thus, we validated our computational predictions, demonstrating TGFβ1 as a master switch controlling expression of SFRP1 and myofibroblast markers in primary fibroblasts.

SFRP1 modulates TGFβ1-induced invasion and RHOA activity in patient fibroblasts

Secreted SFRP1 is an inhibitor of the Wnt signalling pathway [28, 29] and regulating tumour cell invasion [30, 31]. We previously identified a transcriptomic signature of collagen-invading lung fibroblasts characterised by a robust reduction in *Sfrp1* expression [32]. In fibrogenesis, activated fibroblasts are thought to migrate into damaged tissue regions to form fibrotic foci. Transplantation experiments in mouse lungs post-bleomycin injury demonstrated superior migratory capacity of *Cthrc1*$^{+}$ myofibroblasts compared to other fibroblast states [1]. To examine SFRP1's role in fibroblast invasion, we siRNA-depleted SFRP1 in pHLFs from four donors and performed collagen invasion assays and transcriptome analyses (figure 7a and b). SFRP1-deficient cells considerably increased their invasive capacity, similar to TGFβ1-treatment, compared to controls (p<0.001) (figure 7c). Surprisingly, combined SFRP1-siRNA and TGFβ1 treatments gave an inverted phenotype abrogating the TGFβ1-induced invasion. Notably, both increased invasion in untreated SFRP1 knockdown cells and reduced invasion in TGFβ1-stimulated ones, were at least partially restored by reconstituting SFRP1, indicating that SFRP1-dependent pathways modulate TGFβ1-driven fibroblast phenotypes (figure 7d). Additionally, direct treatment of invading fibroblasts with SFRP1 decreased their invasiveness (supplementary figure S8).

Bulk transcriptomic analysis of SFRP1-depleted fibroblasts indicated a downregulation of *RHOA*-signalling-related pathways possibly through upregulation of RhoGDI inhibitory signals (figure 7e). We confirmed diminished expression of *RHOA* mRNA (figure 7f) and reduced RHOA-GTPase activity (figure 7g). Additionally, the SFRP1 knockdown induced cell morphology changes towards elongated cell shapes (figure 7h and i). To test how RhoA inhibition affects fibroblast invasion we used the RhoA inhibitor CT04 in SFRP1-depleted and control cells and found that CT04 treatment alone significantly increased cell invasion (figure 7j). However, we did find a small but significant additive effect on cell invasion using CT04 in SFRP1-decificient cells, suggesting that not all of the modulatory effects of SFRP1 on cell invasion strictly depend on the RhoA pathway (figure 7j).

In summary, our loss of function experiments in pHLFs reveal a function of SFRP1 in modulating TGFβ1 induced fibroblast invasion partially *via* regulation of the RHOA pathway.

Discussion

Fibroblasts are master orchestrators of tissue homeostasis, immune reactions and wound healing. We delineated injury-induced activation states of fibroblast lineages with specific niches in peribronchiolar,

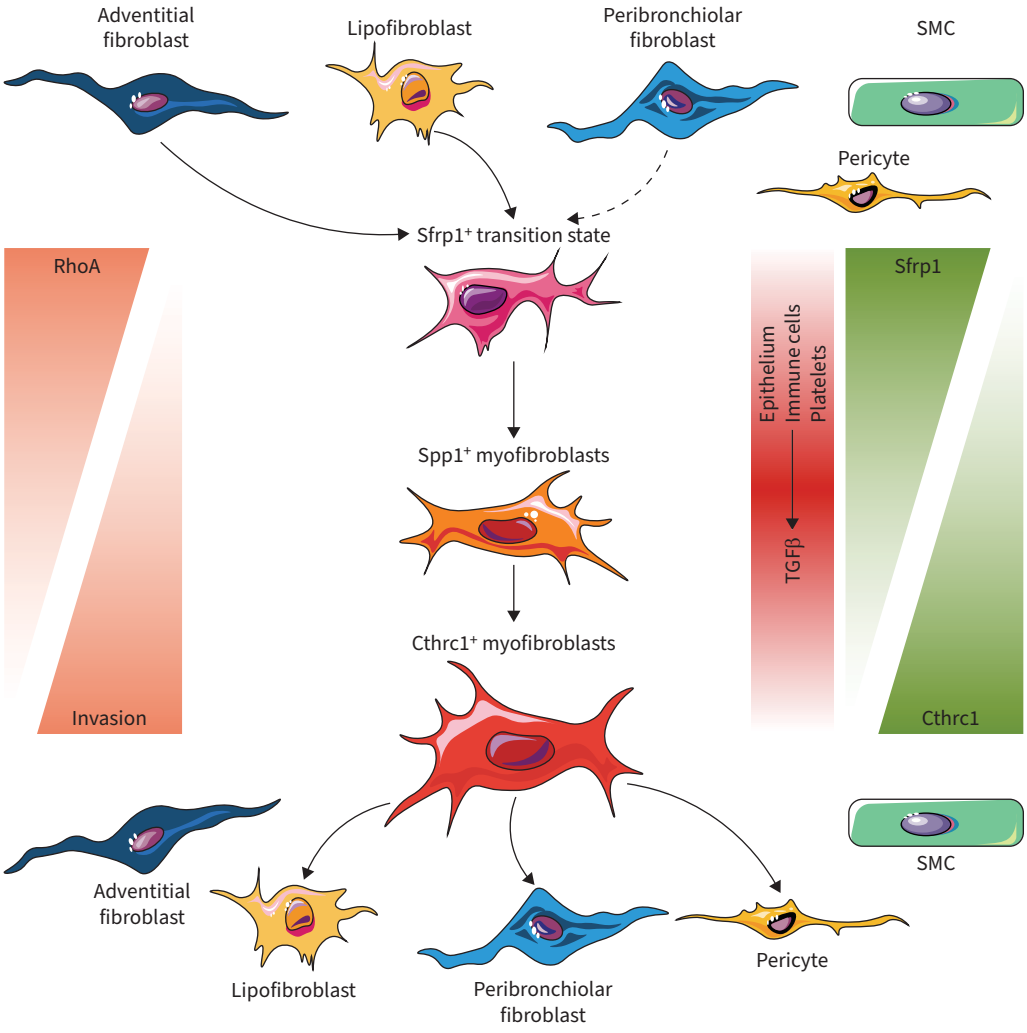

FIGURE 8 Model illustrating fibroblast phenotypic trajectories in lung repair and regeneration. Based on our data we propose the following model of the spatiotemporal evolution of distinct fibroblast states after lung injury. We discovered a novel transitional fibroblast state which is characterised by the expression of Sfrp1, as well as its emergence from adventitial, peribronchial and lipofibroblasts early after injury. Expression of Sfrp1 initially prevents transforming growth factor (TGF)β1 induced fibroblast invasion and RhoA activity. Prolonged exposure to TGFβ1 will in turn lead to increased RhoA activity, cell invasion, downregulation of Sfrp1 expression, and finally induction of the myofibroblast programme, including genes such as ACTA2, SPP1 and CTHRC1. Upon completion of epithelial regeneration, the Cthrc1^{+} myofibroblasts can resolve by differentiation back to a normal homeostatic phenotype. SMC: smooth muscle cell.

adventitial and alveolar lung locations. Longitudinal single-cell and lineage-tracing experiments uncovered a novel transitional cell state and highly cell-type- and lineage-specific paracrine signals mediating specialised functions in lung regeneration. Our analysis further reveals SFRP1 as a key modulator of TGFβ1-induced fibroblast invasion during the myofibroblastic transition in pulmonary fibrosis (figure 8).

The current model of IPF/ILD pathogenesis involves aberrant and/or persistent repair associated with specific (epi-)genetic factors. The bleomycin mouse model likely recapitulates early stages of IPF/ILD pathogenesis more accurately and loses relevance at later stages of disease progression. Indeed, we found interesting similarities of SFRP1^{+} transitional fibroblasts in both early stages after bleomycin injury and mildly affected regions in IPF explants (scored using micro-CT for disease severity). This advocates a high clinical relevance for fibroblast activation states in the bleomycin mouse model mirroring early stages of ILD/IPF.

Our trajectory inference benefits from the very high time resolution after injury (daily sampling) and suggests that adventitial fibroblasts, peribronchiolar and alveolar fibroblasts transcriptionally converge after injury. To our knowledge, this has not been demonstrated before and will require the development of specific genetic lineage tracing tools for experimentally validating our computational predictions. We used single-cell transcriptomics on lungs from the *Tcf*21-Cre reporter mice to address the lineage trajectory of lipofibroblasts. However, a limitation was that all other mesenchymal cell types with exception of the *Hhip*$^+$ peribronchiolar fibroblasts were also lineage-labelled due to low-level *Tcf21* expression. *Tcf21*-lineage-negative *Hhip*$^+$ cells were interestingly heavily expanded after injury. We show that these cells can reside in direct physical contact with AT2 cells and are the exclusive source of morphogens such as *Wnt5a* after injury, which probably has important implications for AT2 progenitor cell function [24].

Previous work established that fibroblast invasion contributes to lung fibrosis progression and severity [1, 33–35]. We here show that the early *Sfrp1*$^+$ transitional state of injury-activated fibroblasts is noninvasive, suggesting that injury-activated fibroblasts serve local niche-functions, like recruiting immune cells by adventitial fibroblasts, or activating epithelial stem cells by lipofibroblasts, pericytes and *Hhip*$^+$ fibroblasts. Our data indicate that recruited myeloid cells, which heavily accumulate early in the bleomycin model [36], plus activated epithelial and lymphatic endothelial cells, produce *Tgfβ* to switch the noninvasive *Sfrp*1$^+$ transitional cells into highly invasive *Cthrc1*$^+$/*Spp1*$^+$ myofibroblasts. Indeed, a profibrotic cell circuit between macrophages and fibroblasts has been described, which requires cadherin-11 mediated direct cell–cell interactions to promote latent TGFβ activation [37].

Interestingly, the classical view of sessile actomyosin based contractile myofibroblasts contradicts our observations of highly invasive and mobile CTHRC1$^+$/ACTA2$^+$ myofibroblasts. Our cell invasion data demonstrate that availability of SFRP1 in pHLFs dictates whether TGFβ1 induces pro-invasive or anti-invasive behaviour. This interesting crosstalk of SFRP1 and TGFβ1 signalling may enable precise timing of distinct fibroblast functions (*e.g.* invasion *versus* ECM remodelling and contraction) during the highly concerted tissue repair post-injury. In pathologies like IPF, myofibroblasts invade to organise themselves into dense accumulations called fibroblast foci, a process which is also recapitulated in the bleomycin model [34]. One limitation of the current study was the uncertainty regarding the commercial anti-SFRP1 antibodies' capacity to neutralise SFRP1 activity. Thus, the mechanisms discovered in this study have direct implications for IPF opening ways for new therapeutic interventions to limit or reverse fibroblast foci formation.

Acknowledgements: We gratefully acknowledge the provision of human biomaterial (primary fibroblasts) and clinical data from the CPC-M bioArchive and its partners at the Asklepios Biobank Gauting, the LMU Hospital and the Ludwig-Maximilians-Universität München. We thank the patients and their families for their support. We are grateful to M. Neumann and A. van den Berg (Comprehensive Pneumology Center (CPC), Munich, Germany) for providing superb technical support. We also thank Inti Alberto de la Rosa Velazquez and the team from the genomics core facility of Helmholtz Munich for expert sequencing service.

Author contributions: Conceptualisation and supervision: G. Burgstaller and H.B. Schiller. Methodology and investigation: C.H. Mayr, A. Sengupta, M. Ansari, J.C. Pestoni, P. Ogar, I. Angelidis, I.E. Fernandez, A. Liontos, J.A. Rodriguez-Castillo, N.J. Lang, M. Strunz, S. Asgharpour, D. Porras-Gonzalez, B. Oehrle, V. Viteri-Alvarez, M. Irmler, M. Tallquist, M. Gerckens, R.M. Wasnick and K. Ahlbrecht. Bioinformatic analysis and software: C.H. Mayr, M. Ansari and F.J. Theis. Surgical work and human tissue: G.M. Stoleriu, J. Behr, N. Kneidinger, W.A. Wuyts and L.J. De Sadeleer. Visualisation and writing: H.B. Schiller, G. Burgstaller, C.H. Mayr, A. Sengupta and R.M. Wasnick. Resources and funding: H.B. Schiller, G. Burgstaller, O. Eickelberg, A.Ö. Yildirim, F.J. Theis, R.E. Morty and C. Samakovlis.

Conflict of interest: M. Gerckens reports grants from Stiftung Atemweg e.V. and a patent pending EP21178481 "Novel anti-fibrotic drugs", outside the submitted work. M. Tallquist reports support for the present manuscript from NIH (5R21HL156112). J. Beckers reports funding for the current manuscript, as well as funding for consumables outside the submitted work, from Helmholtz Zentrum München GmbH. O. Eickelberg reports support for the present manuscript from R01 HL146519; in addition, O. Eickelberg reports consulting fees from Blade Therapeutics, Yap Therapeutics and Pieris Pharmaceuticals, stock or stock options from Blade Therapeutics, outside the submitted work. J. Behr reports a leadership role as Chair of Guideline Committee of the German Respiratory Society (DGP), outside the submitted work. W.A. Wuyts reports grants, consulting fees, lecture honoraria and advisory board participation from Roche, Pliant, Boehringer Ingelheim, Alentis and Galapagos. K. Ahlbrecht reports support for the present manuscript from Max Planck Society, German Center for Lung Research (Deutsches Zentrum für Lungenforschung; DZL), Federal Ministry of Higher Education, Research and

the Arts of the State of Hessen LOEWE, Programme through grant UGMLC; in addition, K. Ahlbrecht reports grants from Rhon Klinikum AG (grant FI_71), outside the submitted work. R.E. Morty reports leadership roles as Editor-in-Chief, *American Journal of Physiology – Lung Cellular and Molecular Physiology* and Group Chair, Group 07.08 Lung and Airway Development, at the European Respiratory Society, outside the submitted work. C. Samakovlis reports grants from Swedish Research Council, Swedish Cancer Society, DFG, Stockholm University, Stockholm, Sweden, Justus-Liebig University, Giessen, Germany, DiscovAir, EU, payment for expert testimony from Swedish Cancer Society and Wallengberg Foundation, and a leadership role with Royal Academy of Science, Sweden, outside the submitted work. F.J. Theis reports support for the present manuscript from the Chan Zuckerburg Foundation (grant number 2019- 002438), as well as consulting fees from Roche, Immunai, Singularity, Omniscope and CytoReason, lecture honoraria from Genentech Research Organisation, AMGEN GmbH, Munich, Roche Germany, Roche, Basel, ETH Zurich, Vizgen, ThirdRockVentures and Pfizer, advisory board participation with Max Planck Institute for Intelligent Systems, Berlin Institute of Health and EMBL, and stock or stock options from Cellarity, outside the submitted work. H.B. Schiller reports support for the present manuscript from Helmholtz Association, Deutsches Zentrum für Lungenforschung (DZL) and CZI/H2020 (discovair). The remaining authors have no potential conflicts of interest to disclose.

Support statement: We acknowledge support by the German Center for Lung Research (DZL), the Helmholtz Association, the European Union's Horizon 2020 research and innovation programme (grant agreement 874656) and the Chan Zuckerberg Initiative (CZF2019-002438). Funding information for this article has been deposited with the Crossref Funder Registry.

References

1 Tsukui T, Sun K-H, Wetter JB, *et al.* Collagen-producing lung cell atlas identifies multiple subsets with distinct localization and relevance to fibrosis. *Nat Commun* 2020; 11: 1920.
2 Zepp JA, Zacharias WJ, Frank DB, *et al.* Distinct mesenchymal lineages and niches promote epithelial self-renewal and myofibrogenesis in the lung. *Cell* 2017; 170: 1134–1148.
3 Xie T, Wang Y, Deng N, *et al.* Single-cell deconvolution of fibroblast heterogeneity in mouse pulmonary fibrosis. *Cell Rep* 2018; 22: 3625–3640.
4 Lee J-H, Tammela T, Hofree M, *et al.* Anatomically and functionally distinct lung mesenchymal populations marked by Lgr5 and Lgr6. *Cell* 2017; 170: 1149–1163.
5 Riccetti M, Gokey JJ, Aronow B, *et al.* The elephant in the lung: integrating lineage-tracing, molecular markers, and single cell sequencing data to identify distinct fibroblast populations during lung development and regeneration. *Matrix Biol* 2020; 91–92: 51–74.
6 El Agha E, Moiseenko A, Kheirollahi V, *et al.* Two-way conversion between lipogenic and myogenic fibroblastic phenotypes marks the progression and resolution of lung fibrosis. *Cell Stem Cell* 2017; 20: 571.
7 Kheirollahi V, Wasnick RM, Biasin V, *et al.* Metformin induces lipogenic differentiation in myofibroblasts to reverse lung fibrosis. *Nat Commun* 2019; 10: 2987.
8 Hung C, Linn G, Chow Y-H, *et al.* Role of lung pericytes and resident fibroblasts in the pathogenesis of pulmonary fibrosis. *Am J Respir Crit Care Med* 2013; 188: 820–830.
9 Frangogiannis N. Transforming growth factor-β in tissue fibrosis. *J Exp Med* 2020; 217: e20190103.
10 Hinz B, Lagares D. Evasion of apoptosis by myofibroblasts: a hallmark of fibrotic diseases. *Nat Rev Rheumatol* 2020; 16: 11–31.
11 Biasin V, Crnkovic S, Sahu-Osen A, *et al.* PDGFRα and αSMA mark two distinct mesenchymal cell populations involved in parenchymal and vascular remodeling in pulmonary fibrosis. *Am J Physiol Lung Cell Mol Physiol* 2020; 318: L684–L697.
12 Sun K-H, Chang Y, Reed NI, *et al.* α-Smooth muscle actin is an inconsistent marker of fibroblasts responsible for force-dependent TGFβ activation or collagen production across multiple models of organ fibrosis. *Am J Physiol Lung Cell Mol Physiol* 2016; 310: L824–L836.
13 Park J, Ivey MJ, Deana Y, *et al.* The Tcf21 lineage constitutes the lung lipofibroblast population. *Am J Physiol Lung Cell Mol Physiol* 2019; 316: L872–L885.
14 Travaglini KJ, Nabhan AN, Penland L, *et al.* A molecular cell atlas of the human lung from single-cell RNA sequencing. *Nature* 2020; 587: 619–625.
15 Angelidis I, Simon LM, Fernandez IE, *et al.* An atlas of the aging lung mapped by single cell transcriptomics and deep tissue proteomics. *Nat Commun* 2019; 10: 963.
16 Kuppe C, Ibrahim MM, Kranz J, *et al.* Decoding myofibroblast origins in human kidney fibrosis. *Nature* 2021; 589: 281–286.
17 Kadur Lakshminarasimha Murthy P, Sontake V, Tata A, *et al.* Human distal lung maps and lineage hierarchies reveal a bipotent progenitor. *Nature* 2022; 604: 111–119.
18 Sountoulidis A, Liontos A, Nguyen HP, *et al.* SCRINSHOT enables spatial mapping of cell states in tissue sections with single-cell resolution. *PLoS Biol* 2020; 18: e3000675.

19 Schiller HB, Fernandez IE, Burgstaller G, *et al.* Time- and compartment-resolved proteome profiling of the extracellular niche in lung injury and repair. *Mol Syst Biol* 2015; 11: 819.
20 Mayr CH, Simon LM, Leuschner G, *et al.* Integrative analysis of cell state changes in lung fibrosis with peripheral protein biomarkers. *EMBO Mol Med* 2021; 13: e12871.
21 Lange M, Bergen V, Klein M, *et al.* CellRank for directed single-cell fate mapping. *Nat Methods* 2022; 19: 159–170.
22 Davis MN, Horne-Badovinac S, Naba A. *In-silico* definition of the *Drosophila melanogaster* matrisome. *Matrix Biol Plus* 2019; 4: 100015.
23 Klingberg F, Hinz B, White ES. The myofibroblast matrix: implications for tissue repair and fibrosis. *J Pathol* 2013; 229: 298–309.
24 Nabhan AN, Brownfield DG, Harbury PB, *et al.* Single-cell Wnt signaling niches maintain stemness of alveolar type 2 cells. *Science* 2018; 359: 1118–1123.
25 Ding L, Dolgachev V, Wu Z, *et al.* Essential role of stem cell factor-c-Kit signalling pathway in bleomycin-induced pulmonary fibrosis. *J Pathol* 2013; 230: 205–214.
26 Browaeys R, Saelens W, Saeys Y. NicheNet: modeling intercellular communication by linking ligands to target genes. *Nat Methods* 2020; 17: 159–162.
27 Hu B, Wu Z, Bai D, *et al.* Mesenchymal deficiency of Notch1 attenuates bleomycin-induced pulmonary fibrosis. *Am J Pathol* 2015; 185: 3066–3075.
28 He J, Sheng T, Stelter AA, *et al.* Suppressing Wnt signaling by the hedgehog pathway through sFRP-1. *J Biol Chem* 2006; 281: 35598–35602.
29 Gibb N, Lavery DL, Hoppler S. sfrp1 promotes cardiomyocyte differentiation in *Xenopus via* negative-feedback regulation of Wnt signalling. *Development* 2013; 140: 1537–1549.
30 Chen Y-L, Wang T-H, Hsu H-C, *et al.* Overexpression of CTHRC1 in hepatocellular carcinoma promotes tumor invasion and predicts poor prognosis. *PLoS One* 2013; 8: e70324.
31 Baharudin R, Tieng FYF, Lee L-H, *et al.* Epigenetics of *SFRP1*: the dual roles in human cancers. *Cancers* 2020; 12: 445.
32 Oehrle B, Burgstaller G, Irmler M, *et al.* Validated prediction of pro-invasive growth factors using a transcriptome-wide invasion signature derived from a complex 3D invasion assay. *Sci Rep* 2015; 5: 12673.
33 Ahluwalia N, Grasberger PE, Mugo BM, *et al.* Fibrogenic lung injury induces non-cell-autonomous fibroblast invasion. *Am J Respir Cell Mol Biol* 2016; 54: 831–842.
34 Tsukui T, Ueha S, Abe J, *et al.* Qualitative rather than quantitative changes are hallmarks of fibroblasts in bleomycin-induced pulmonary fibrosis. *Am J Pathol* 2013; 183: 758–773.
35 Li Y, Jiang D, Liang J, *et al.* Severe lung fibrosis requires an invasive fibroblast phenotype regulated by hyaluronan and CD44. *J Exp Med* 2011; 208: 1459–1471.
36 Strunz M, Simon LM, Ansari M, *et al.* Alveolar regeneration through a $Krt8^{+}$ transitional stem cell state that persists in human lung fibrosis. *Nat Commun* 2020; 11: 3559.
37 Lodyga M, Cambridge E, Karvonen HM, *et al.* Cadherin-11-mediated adhesion of macrophages to myofibroblasts establishes a profibrotic niche of active TGF-β. *Sci Signal* 2019; 12: eaao3469.